Silver-Nanoparticle-Conjugated Polypeptide Brushes for Surface-Enhanced Raman Scattering

Di-Yan Wang,[†] Tzu-Shen Teng,[†,‡] Yi-Chou Wu,[†] Yi-Cheng Lee,[‡] Kuei-Hsien Chen,[§] Chung-Hsuan Chen,[‡] Ying-Chih Chang,*[,‡] and Chia-Chun Chen*[,†,§]

Department of Chemistry, National Taiwan Normal University, Taipei, Taiwan, Taipei 116, Taiwan, The Genomics Research Center, Academia Sinica, Taipei 115, Taiwan, and Institute of Atomic and Molecular Sciences, Academia Sinica, Taipei 106, Taiwan

Received: April 21, 2009; Revised Manuscript Received: June 10, 2009

A soft surface-enhanced Raman scattering (SERS) substrate was fabricated based on a three-dimensional (3D) structure of biocompatible end-tethered poly(L-lysine) ("t-PLL") with a brushlike configuration conjugated with silver nanoparticles (Ag NPs) (Ag NP-t-PLL film). The conjugation procedures were carefully adjusted to generate the films with different interval widths (*W*) between Ag NPs and diameters (*D*) of Ag NPs. The resulting film was then characterized by zeta potential, CD spectropolarimeter, and scanning electron microscopy. Furthermore, the studies of SERS enhancements using Ag NP-t-PLL film as a substrate were performed. The significant increases of SERS enhancements have been obtained as *W*/*D* was decreased from 0.9 to 0.2. Our results not only afford a facile fabrication of a 3D soft substrate for SERS with high sensitivity and biocompatibility but also offer great potentials for the development of new biosensors.

1. Introduction

Surface-enhanced Raman scattering (SERS) of organic molecules adsorbed on metal NPs has been intensively explored in experimental and theoretical aspects recently.[1−9] Many great efforts have been made to increase the detection limit of SERS signal of analyte concentration.[5,6] For instance, the SERS sensitivity of Rhodamine 6G (R6G) molecules adsorbed on silver NPs (Ag NPs) has been reached to $\sim 1 \times 10^{-15}$ M.[5] In comparison to fluorescence spectra, SERS spectra can provide not only the optical properties of adsorbed molecules but also their structural fingerprints.[6,10] Therefore, one of the important SERS applications is for the identification on trace biological molecules without fluorescence signal such as DNA and RNA.[11,12] Recent studies have shown that detection DNA or RNA have been performed dye-labeled oligonucleotide sequences in a quantitative manner[13,14] and resolved label-free direct identification of mononucleotides in low concentration aqueous solution.[11] Furthermore, SERS techniques have exhibited great potentials for the understanding on some biological activities such as rapid and ultrasensitive determination of enzyme activities,[15] characterization of a number of species and strains of bacteria,[16] and even direct detection of cancer cells as a potential diagnostic maker.[17] New biological applications of SERS are being explored.

A soft substrate is required in order to study biological activities of living cells or species by SERS. The technical challenge for the fabrication of an adaptable substrate is to load metal NPs properly onto the biocompatible materials on the surface. Two main factors should be controlled carefully in order to reach the optimization, reliability and reproducibility of Raman signal. First, the growth of metal NPs directly on a soft substrate has increased the difficulty in controlling the sizes and shapes of resulting NPs. Thus, the maximized SERS signal is difficult to obtain because the signal enhancements have exhibited dependencies on the size[18,19] and shape[20,21] of NPs. Second, to reach the maximized SERS enhancement, it is necessary to adjust the ratio (*W*/*D*) of nanoparticle diameter (*D*) and interval width (*W*) between NPs on substrates. The great SERS enhancement has been reported while significant near-field interaction occurs between adjacent Ag nanorods with their *W* reaching half the value of their diameter.[9] Of recent, different types of SERS substrates have been fabricated by the controlled growth, conjugation or assembly of metal NPs on the surface. For examples, the porous anodic aluminum oxide (AAO) deposited with Ag NPs has been utilized as a SERS substrate.[22] The *W* and *D* of the NPs have been controlled through the hole and wall thickness of AAO during the conjugation of Ag. The monolayers of aligned Ag nanowires are assembled by using the Langmuir−Blodgett technique on a silicon wafer to generate a suitable SERS substrate.[23] Also, the silicon nanotips with Ag NPs on the tip for SERS measurements is fabricated by ion sputtering technique.[24] Besides the metal NPs on an inorganic substrate, they can be also directly grown and deposited onto biocompatible materials such as polymers,[25−31] polypeptides,[1,5] and mononucleotides[13] on the substrate surface. For example, dendrimer/metallic NPs are deposited on the surface to form a layer-by-layer film as a SERS substrate.[25] A high-density nanoparticle film has been fabricated for SERS measurements using polymers as a template.[26] In this study, the spacing between NPs is adjusted by generating the polymer swelling and shrinkage through the control of temperature. In spite of the polymers, 3-amine propyl-triethoxysilane (APS) dispersed on a glass slide has usually been exploited as a SERS substrate for probing biological molecules on the unique gold nanoparticle aggregates.[32] In addition, the studies of SERS detection for micro-organisms have also been reported using different types of substrates such as Au NP-coated SiO_2,[16] metalized nanostructured poly(*p*-xylylene) films,[28] and codeposited bacteria and Ag on an inert surface.[33] But practical SERS probes for

* Corresponding author. E-mail: cjchen@ntnu.edu.tw (C.-C.C); yingchih@gate.sinica.edu.tw (Y.-C.C.).
† National Taiwan Normal University.
‡ The Genomics Research Center, Academia Sinica.
§ Institute of Atomic and Molecular Sciences, Academia Sinica.

10.1021/jp903664u CCC: $40.75
Published on Web 07/02/2009

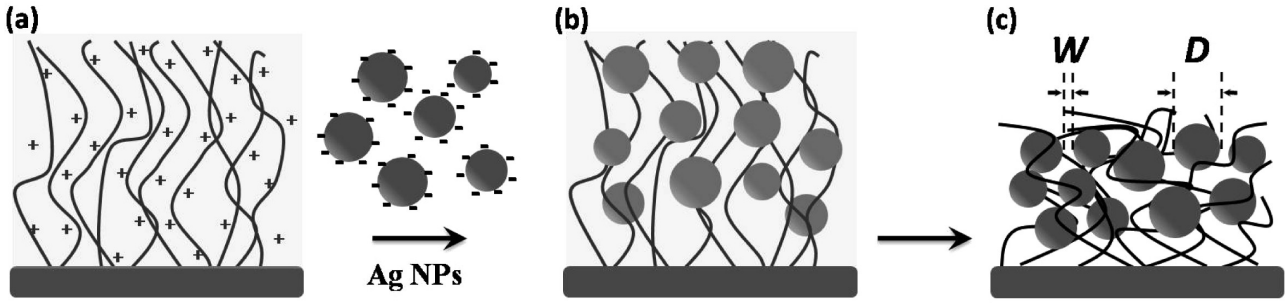

Figure 1. Schematic illustration of the fabrication of Ag NP-t-PLL film. (a) The amine groups of PLL chains of the t-PLL brush exposed positive charges in Ag NPs solution. The negatively charged Ag NPs were conjugated onto the film via strong electrostatic interaction and thus the (b) Ag NP-t-PLL film in solution was formed. The film was removed from Ag NPs solution and then washed by deionized water. After the film was dried, (c) the Ag NP-t-PLL film was prepared, and the *W* and *D* of Ag NP-t-PLL film were also defined. The *W*/*D* of Ag NP-t-PLL film was varied as the different conjugation conditions were applied.

biological applications have not been well-developed because of some difficulties in preparing robust and uniform SERS substrates that provide maximum SERS enhancement. Up to date, the developments of a large active area as a soft SERS substrate are still needed for future applications on the studies of cell or bacteria activities.

The film of poly(L-lysine) (PLL) has been widely used for cell cultures. In our previous works,[34−36] we have developed 3D structure of end-tethered poly(L-lysine)" ("t-PLL") with a brushlike configuration onto silicon oxide surfaces. The stimuli-responsive properties of t-PLL brush are demonstrated by the dielectric property changes while converting among α-helix, *β*-sheet, and random coil. The pH (H^+/OH^-), surfactant (SDS), and anion (ClO_4^-) are chosen as the external stimuli.[35] In addition, PLL is an important water-soluble polypeptide composed of naturally L-lysine-including amine groups on the side chains. It is also a necessary building block for all protein in the body. It shows a great biological application on cell culture as the coating materials on the surface of cell culture disk.[37]

In this paper, we fabricated a soft SERS substrate based on a three-dimensional (3D) structure of biocompatible t-PLL brush conjugated with Ag nanoparticles (Ag NP-t-PLL film) (Figure 1). The zeta potential, CD spectropolarimeter and scanning electron microscopy were performed to characterize the films. By the adjustments of conjugation procedures, the resulting Ag NP-t-PLL films with different *W* and *D* were obtained. Furthermore, the effects on SERS enhancements by the *W*/*D* were discussed.

2. Experimental Section

Synthesis of t-PLL Brush. The t-PLL brush on the amine-modified planar substrates was prepared by following the previous method[35] with some modifications. In brief, poly(N^ε-carbobenzyloxy-L-lysine) (PCBL), the precursors of t-PLL, were grown from the amine-modified (APS) solid substrates (APS monolayer) by SI-VDP of the N-carboxyanhydride (NCA) of N^ε-carbobenzyloxy-L-lysine (CBL) at a 102 °C substrate temperature and NCA evaporating temperature, 1.0×10^{-5} to 1.0×10^{-6} Torr, and a 1 h reaction time. Other reaction parameters including the amount of NCA, substrate temperature, and reaction time were optimized for the PCBL system. After the SI-VDP reaction was completed, the substrates were sonicated in a mixture of dichloroacetic acid (DCA) and chloroform (20/80 (v/v)) for 5 min, followed by rinsing with fresh chloroform and drying under a stream of nitrogen. To converse PCBL to t-PLL, the PCBL films were sonicated in the HBr/benzene solution for 40 min to remove N^ε-carbobenzyloxy protection groups. After the reaction, the substrates were rinsed with toluene, acetone, and distilled water and dried under a stream of nitrogen. The thickness of the t-PLL brush was controlled by the reaction time of SI-VDP. In this report, we have prepared the t-PLL brushes with different thickness of ∼34, 47, and 70 nm. The thickness of t-PLL brushes were measured using a conventional Gaertner Stokes ellipsometer LSE with a He−Ne laser ($\lambda = 632.8$ nm) and a fixed incident angle of 70°. The film thickness and refractive index were calculated using the Gaertner Ellipsometer Measurement Program.

Synthesis of Au and Ag NPs. Synthesis of Au NPs: The initial solution was prepared by mixing 0.5 mL of $HAuCl_4$ (10 mM), 0.5 mL of trisodium citrate (0.5 mM), and 18 mL of deionized water into a vial. Next, 1 mL of ice cold $NaBH_4$ solution (0.1 M) was added to the solution all at once while stirring. The solution turned pink and then a reddish color, indicating that Au NPs were formed successfully.

Synthesis of Ag NPs: A solution of 2 mL of $AgNO_3$ (1 mM) and 2 mL of trisodium citrate (1 mM) was added with 1 mL of ice cold 0.1 M $NaBH_4$ solution at once while stirring. The resulting solution turned yellow while Ag NPs were formed. The as-prepared Ag NP solution was added to sodium citrate to adjust the pH values, forming the three solutions of Ag NPs with pH 5, 7, and 9. The absorption spectra of Au and Ag NPs were confirmed by absorption spectra recorded using a HP 8453 UV−vis spectrometer.

Preparation of the Ag NP-t-PLL Films. Syntheses of Ag NP-t-PLL films: The Ag NPs solutions with pH 5, 7, and 9 were added separately into vials with t-PLL brushes (the thickness about 47 nm). After 1 h, Ag NP-t-PLL films were formed. Also, the t-PLL brushes with the thicknesses of 34 and 70 nm were placed into vials separately. Afterward, the Ag NP solutions with pH 5 (20 mL) were added to each vial, resulting in Ag NP-t-PLL films. Besides, for adjusting the total immersion time, the three t-PLL brushes (thickness ≈ 70 nm) immersed in the Ag NPs solution with pH 5 for 1, 2, and 4 h, respectively.

To investigate the surface charge of Ag NPs and t-PLL brush, we measured the zeta potential of Ag NPs and t-PLL brush by Zetasizer instrument in pH 3−9 buffers. The CD spectra of Ag NP-t-PLL film on quartz were measured by JASCO J-60 spectropolarimeter to examine the conformation of Ag NP-t-PLL film in pH 6, 9, and 11 buffers. For configuration analysis, all of the SEM (JEOL-JSM-6700F) images were inspected with a platinum coating. To take the cross-sectional SEM image, a custom sample holder with 1 cm depth groove was used, and the substrate was tilted vertically and stuck on the side wall of the groove.

Raman Spectroscopy Measurements. R6G solution was diluted to various concentrations ranging from 1×10^{-6} to $1 \times$

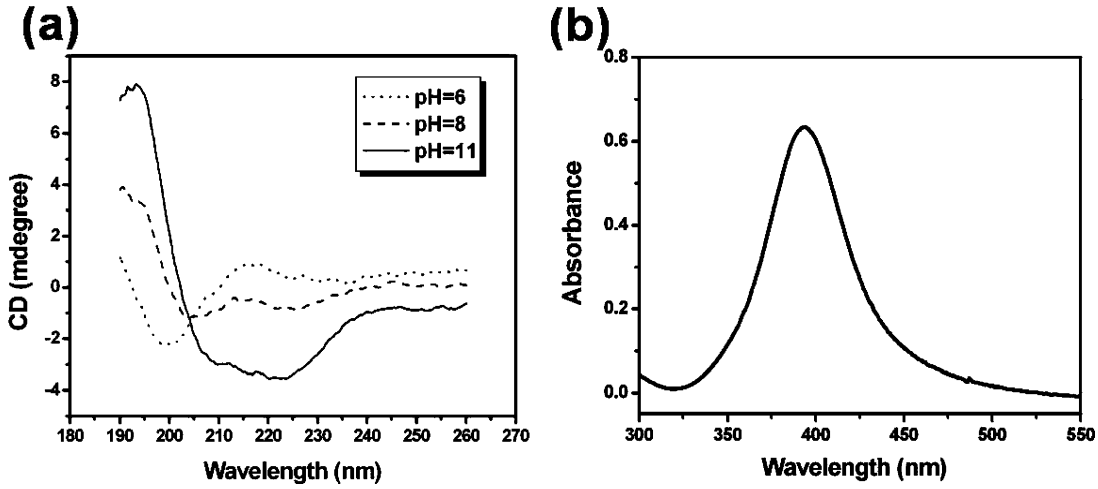

Figure 2. (a) CD spectra of a t-PLL brush on a quartz plate in buffer pH 6, 8, and 11. (b) UV−vis spectra of Ag NPs exhibited a SPR absorption peak at ∼390 nm.

10^{-9} M with methanol and dropped onto our metal NP-t-PLL films. After the solvent was allowed to evaporate under ambient conditions, these films were then used for the Raman measurements using a Raman spectrometer of Jobin Yv on-LabRAM HR800. The excitation source is an argon laser (514 nm). The diameter of focused laser spot on the sample is 1 μm. The power of the laser light is about 10 mW and the integrated time of Raman spectra is 5 s. For increasing the reliable extent of SERS enhancement related to the Ag NP-t-PLL films, each of Raman spectra is the average of nine Raman spectra on different locations of the same substrate.

3. Results and Discussion

3.1. Preparation and Characterization of t-PLL Brushes and Ag NPs. t-PLL brush was prepared by the surface-initiated vapor-deposition polymerization (SI-VDP) as described in the experimental section. Figure 2a showed the CD spectra of resulting t-PLL brushes on the quartz substrate in an aqueous solution while the pH of the solution was varied from 6 to 11. At pH 6, the CD spectrum of t-PLL brush exhibited a maximum centered at 217 nm and a minimum at 198 nm. The results suggested that t-PLL brush was under random-coil conformation according to the previous studies.[35] As the pH was adjusted to 11, the CD spectrum showed double minimum peaks at 210 and 222 nm, and a maximum at 193 nm, which were typical absorption peaks for the α-helical conformation of PLL. Our results indicated that conformation of the t-PLL brush was altered from the pH 6 to 11. The changes were mainly due to the differences of hydrogen bonding interaction on PLL backbones. For the preparation of Ag NPs, Ag ions were reduced in a sodium citrate solution. The UV−vis spectra (Figure 2b) of as-prepared Ag NPs solutions exhibited a strong absorption peak at 390 nm derived from surface plasmon resonance (SPR) of Ag NPs. The solution was stable over long periods of time because citrates form an outer layer on the surface of the NPs. This ensured a stable surface layer with a negatively charged surface and a stable colloid suspension. The size and size distribution of Ag NPs and Au NPs were measured by TEM before the NPs conjugated with t-PLL brush. The results showed that the averaged diameter of Ag NPs and Au NPs were ∼15 and ∼20 nm, respectively. The size distributions of Ag NPs and Au NPs were in the range of 5−25 nm and 15−25 nm, respectively.

The pH of Ag NPs solution and t-PLL brush was changed from 4 to 9 and 3 to 9, respectively, in order to adjust the

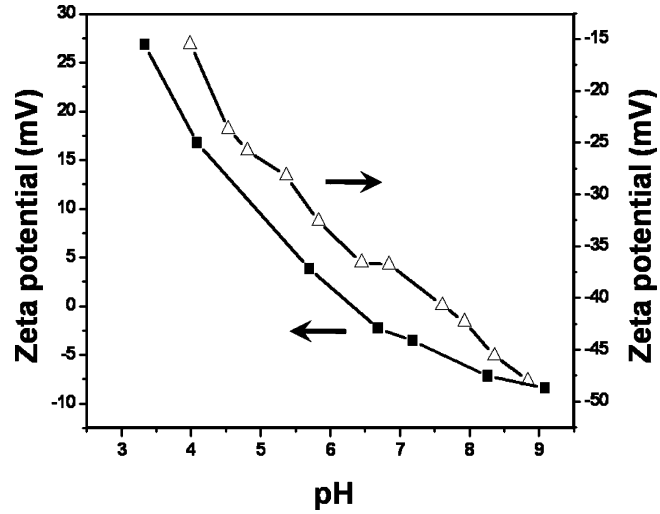

Figure 3. pH dependence of the zeta potential of Ag NPs (open triangles) and t-PLL brush (filled squares).

electrostatic forces between t-PLL brush and Ag NPs when the t-PLL brush was immersed into the solution. The zeta potential measurements were performed to determine the surface charges of t-PLL brush and Ag NPs (Figure 3). The zeta potential of Ag NPs modified with the anion surfactant sodium citrates was −15.5 mV at pH 4. The result indicated that the surface charge of the Ag NPs was negative. When the pH value of the buffer solution was increased to 8.85, the zeta potential was reduced to −48 mV. Generally, the negative surface charge of the Ag NPs was increased with the increases the pH values. But the aggregation of Ag NPs was found in the Ag NPs solution under pH < 5 due to the strong interaction of citrate layer on NPs surface and ions in buffer. The surface of t-PLL brush exhibited positive surface charge under pH < 7. Whereas the aqueous solution reached to neutral, the zeta potential of t-PLL brush was close to zero. Apparently, the surface charge of t-PLL brush and Ag NPs were opposite when the solution was kept at pH 5−7 based on the zeta potential measurements. Because of their opposite charges, the binding forces between t-PLL brush and Ag NPs were believed to be mainly coming from the electrostatic interaction. Besides, when the pH of the buffer was above 7, the surface of the t-PLL brush reversed to negative charge. The negative charge was coming from the solvation interaction of the amine group of the t-PLL brush with the ions in the buffer at pH > 7.

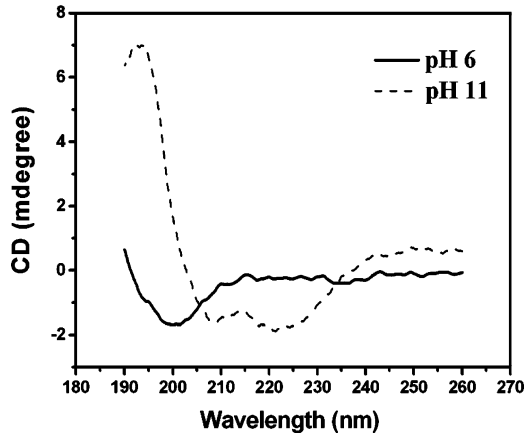

Figure 4. CD spectra of Ag NP-t-PLL films in pH 6 and pH 11 buffer solutions.

3.2. Preparation and Characterization of Ag NPs Conjugated with t-PLL Brushes. ***(a) Conjugation of Ag NPs onto t-PLL Brush.*** The CD spectra of Ag NP-t-PLL films were shown in Figure 4 to verify the conformation of the film. The structure of the films remained a random-coil conformation at pH 6 and an α-helical conformation at pH 11 after the conjugation. SEM measurements of the cross-section of Ag NP-t-PLL films indicated that silver NPs were successfully conjugated into the 3-D structure of t-PLL brushes. In addition, the UV−vis absorption spectra of Ag NP-t-PLL films were measured to verify the conjugation of Ag NPs onto the t-PLL brush. The spectra were recorded after the film was immersed into Ag NPs solution and then stayed for different periods. The results showed that the intensity of Ag plasma absorption peak was increased with the increases of total immersion time, indicating that the amount of Ag NPs of Ag NP-t-PLL film was increased (data not shown). However, under our conjugation conditions, the conformation of t-PLL brush remained even though the amount of Ag NPs was varied.

(b) Variation in D of Ag NPs on Ag NP-t-PLL Film. The Ag NPs have been successfully conjugated with the positively charged t-PLL brush by electrostatic interaction in the range of pH 5 to 9. However, we have found that the average D of Ag NPs of Ag NP-t-PLL film were varied when the t-PLL brush (thickness ∼47 nm) were immersed into Ag NP solutions with different pH. Figure 5a−c showed the scanning electron microscopy (SEM) images of the samples that the films were immersed at pH 5, 7, and 9. Ag NPs of Ag NP-t-PLL films were clearly observed in the images. The distribution of the NPs was quite uniform without aggregation. The average D of Ag NPs on t-PLL brushes were 25, 18, and 10 nm calculated from the SEM images, while the conjugation were performed at pH 5, 7, and 9, respectively. Of interest, the W on the film between neighboring NPs was quite close (5 ± 2 nm) for those three films. Notice that the intensity of SERS has shown strong dependencies on W/D of other types of substrates. The effects of W/D on SERS signal for Ag NP-t-PLL films are discussed below.

(c) Variation in W between Ag NPs on Ag NP-t-PLL Films. The W between individual Ag NPs of the film were different when the thickness of the t-PLL brushes was varied. Figure 5a, d, and e showed the SEM images of three Ag NP-t-PLL films prepared by using t-PLL brushes with different thicknesses at the pH 5. The average W values between Ag NPs on each t-PLL brush were 21 ± 12, 5 ± 2, and 7 ± 3 nm calculated from the SEM images, while the conjugation was performed using t-PLL brushes with the thicknesses of 34, 47, and 70 nm, respectively. The images indicated that the W was reduced with the increases of the thickness of t-PLL brushes (from 34 to 47 nm). However, when the thickness of t-PLL brushes was up to 70 nm, the W increased to 7 ± 3 nm. For the comparison, we have also performed the similar experiments on the APS monolayer. Figure 5f showed that very few Ag NPs has been conjugated with the APS monolayer. A large W of 108 ± 46 nm was obtained in this sample. The result may be attributed to relatively fewer amine groups on the APS monolayer for the NPs conjugation in comparison to t-PLL brushes. Our overall results have indicated that a large number of NP conjugating onto the films usually resulted in a decrease in W. The increases in NP conjugations might be achieved by an increase in the number of amine groups. However, the maximum NP conjugation was obtained at the t-PLL brushes with a thickness of 47 nm under an immersion time of 1 h.

In addition, variations in D or W were also observed when the total immersion time was increased during the preparation (thickness of t-PLL ≈ 70 nm). When the immersion time was increased to 4 h, the intensity of the R6G Raman signal in SERS measurements was enhanced about 4-fold over the immersion time of 1 h (data not shown). It was believed that the amount of Ag NPs in the Ag NP-t-PLL film increased with an increase in total immersion time and may lead to a decrease in W, resulting in an increase in SERS intensity. Our research has shown that the increase in SERS intensity was strongly related to the changes of D and W (see below).

3.3. SERS Enhancement of Ag NP-t-PLL Films. ***(a) Investigation on SERS Enhancement Affected by D and W.*** *Changes in D of Ag NPs.* To explore the correlation between SERS enhancement and D of Ag NPs, we have collected a typical series of 1×10^{-7} M R6G Raman signals (Figure 6) from the samples with a fixed W (5 ± 2 nm) that mentioned above in Figure 5a−c. Clearly, all the peaks of spectra in Figure 5 were assigned to R6G Raman modes such as ν(C−C−C) stretching mode at 614 cm^{-1}, ν(C−H) out-of-plane bend mode at 774 cm^{-1}, ν(C−H) in-plane bend mode at 1129 cm^{-1}, ν(C−C) stretching mode at 1363, 1509, and 1650 cm^{-1}.[38] No significant Raman signal was detected from t-PLL brush. It is most likely due to the inherently small Raman cross-section of the molecule itself with a particular laser excitation (514 nm). The intensity of Raman spectra of R6G molecules at $D = 25$ nm was dramatically higher than that at $D = 10$ and 18 nm. By calculated W/D from the SEM image, the W/D of films at pH 5, 7, and 9 were approximately 0.2, 0.3, and 0.5, respectively. The enhancement at the $W/D \approx 0.2$ was the 3-fold over at the ratio ∼0.3 and 0.5 for the 1363 cm^{-1} band.

Changes in W between Ag NPs. To investigate correlation between SERS enhancement and W/D with the change in W, we have collected a typical series of 1×10^{-7} M R6G Raman signals from the Ag NP-t-PLL films with $W = 21 \pm 12$, 7 ± 3, and 5 ± 2 nm (Figure 7). As the Ag NP-t-PLL film with thin thickness of t-PLL brushes (34 nm) showed a large W, the intensity of Raman signal was rather low. With the increase of thickness of t-PLL brushes (47 nm), the W decreases to 5 ± 2 nm and the SERS intensity increased up to a maximum ∼1811 arb. unit for 1363 cm^{-1}. However, when the thickness of t-PLL brushes increased to 70 nm, the SERS intensity decreased due to increase of W (7 ± 3 nm). In this case, we found that increase of SERS enhancement was related to the reduction of W/D (from 0.95 to 0.2) with fixed D (25 nm). However, when SERS was performed on the Ag NPs conjugated with APS monolayer on

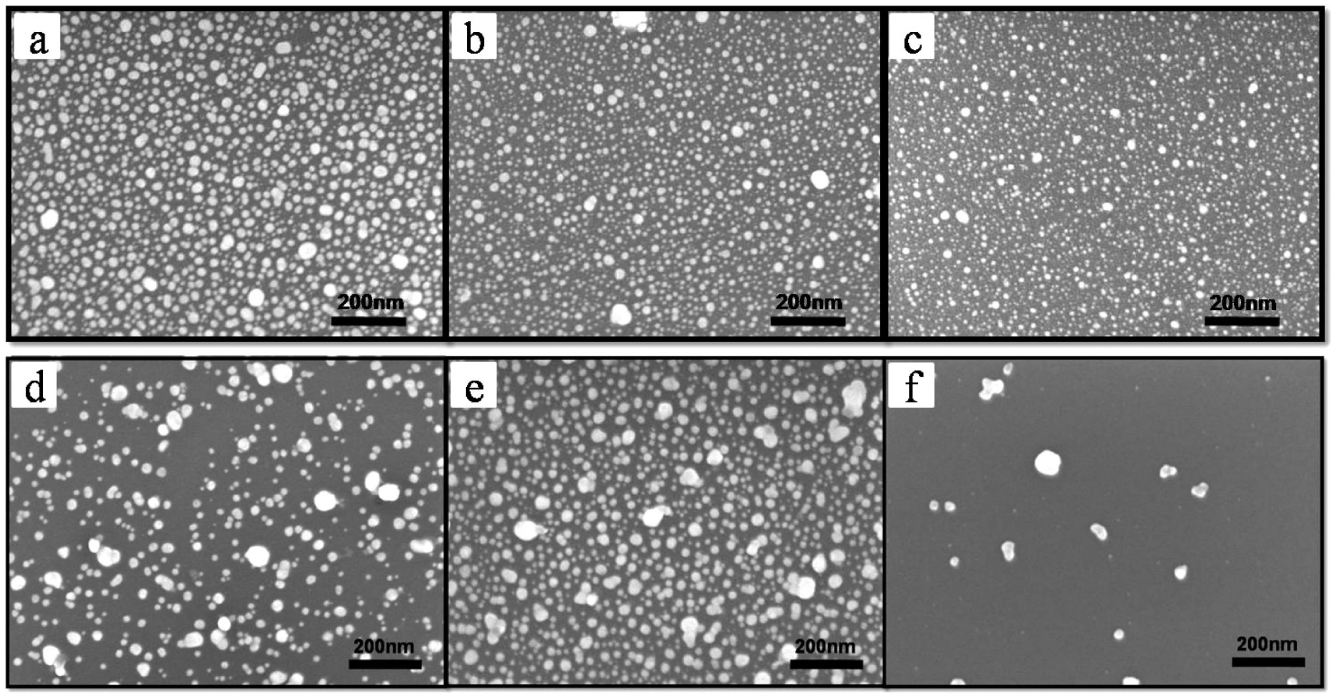

Figure 5. SEM images of the t-PLL brushes and APS monolayer conjugating with Ag NPs. When the t-PLL brushes (thickness ≈ 47 nm) were immersed into Ag NPs solutions with (a) pH 5, (b) pH 7, and (c) pH 9, the average *D* of Ag NPs of Ag NP-t-PLL films were varied. Besides, when the t-PLL brushes with thickness of (d) 34 and (e) 70 nm were immersed in the Ag NPs solution with pH 5, the *W* between Ag NPs on the film were different. (f) When APS monolayer was immersed into Ag NPs solution with pH 5, a large *W* was obtained. (Immersion time of all samples is 1 h).

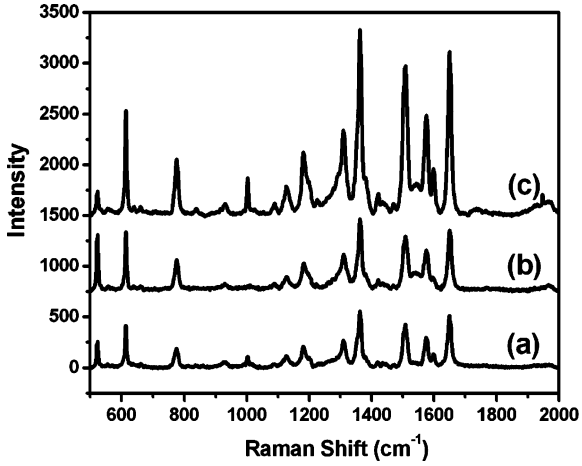

Figure 6. SERS spectra of 1×10^{-7} M R6G were measured on three Ag NP-t-PLL films with *D* values of (a) 10, (b) 18, and (c) 25 nm.

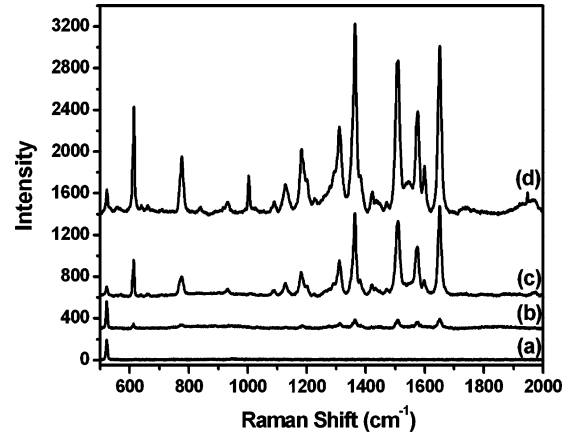

Figure 7. SERS spectra of 1×10^{-7}M R6G were measured on the films with *W* values of (a) 108 ± 46, (b) 21 ± 12, (c) 7 ± 3, and (d) 5 ± 2 nm.

the silicon substrate, no SERS signal was observed because of the few Ag NPs on the substrate with a large *W* (108 nm).

Effects of W/D on SERS Enhancements. Figure 8 showed that threshold behavior of the enhancement of Raman intensity depended primarily on *W/D* with the changes of either *W* or *D*. The result demonstrated that a decrease in *W/D* resulted in a clear increase in the recorded SERS intensity. At first, when *W/D* was reduced below 0.95, the Raman signals increased slowly, then becoming significantly stronger at $W/D = 0.5$, and finally showing a dramatic enhancement when *W/D* reached a ratio of 0.2. Previously, the dependencies of the SERS enhancement on *W/D* have been studied in other types of substrates conjugated with metal NPs. For instances, the theoretical calculations have indicated that SERS signals depend on gap between Ag NPs ($D = 10$ nm) arranged in a linear chain by using a full-scale analytic solution.[8] The studies also indicate that the enhancement at the $W/D \approx 0.25$ is the 3.7-fold over at the ratio ~0.5. Besides, other theoretical predictions by García-Vidal and Pendry,[9] have also shown that the enhancement at $W/D \approx 0.25$ is 7-fold over at the ratio ~0.5, using an array of semicircular Ag nanorods as a calculation model. Experimentally, the SERS measurements have been performed on the arrays of Ag NPs grown in AAO nanochannels with a precisely controlled variation of *W/D*.[22] The experimental results indicate that as $W/D < 1$, the Raman peaks increase in intensity, slowly at first, then becoming significantly stronger at the ratio reaching 0.4. Furthermore, as the *W/D* reaches 0.2, the intensity of Raman spectra reveals the dramatic enhancement (about 5-fold compared to $W/D = 0.5$). In other experimental result, the close-packed Au NPs arrays with different diameters have been fabricated on ITO glass and shown that with the increase of the diameters of the Au NPs, the Raman enhancement increases and reaches a maximum for 25 nm.[39] Our experimental results

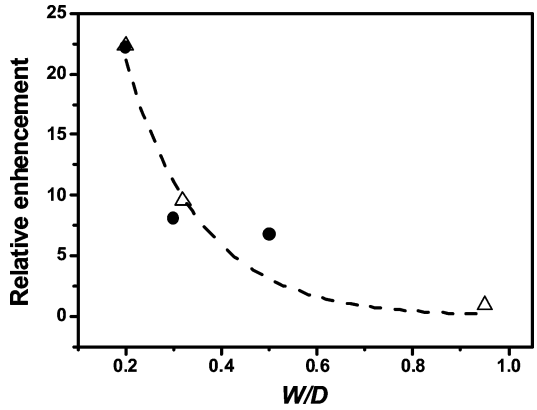

Figure 8. Relative enhancement versus *W*/*D* with change of *W* (open triangles) and change of *D* (filled circles) quantified as I^{SERS} $(W/D)/I^{SERS}$ $(W/D)^{max}$. I^{SERS} represented that the intensity of SERS signal of R6G molecules measured from the Ag NP-t-PLL films with different *W*/*D*. The dashed line is a guide to the eyes.

above showed the similar trend in comparison to those previous theoretical calculations and experimental measurements.

Several previous works have indicated that the increases in SERS intensity are mainly due to the amplification of electromagnetic field between metal NPs.[1−6] In our works, the enhancements of electromagnetic field of Ag NPs of Ag NP-t-PLL films were achieved by the decreases in *W* or the increases in *D*. As the Ag NPs arrange in close proximity to each other (the decreases of *W*), the transition dipoles of the NPs couple to each other. The enhanced magnetic fields of each nanoparticle begin to coherently interfere at the junction sites (also called as hot spots) between NPs.[40,41] Therefore, the decreases in *W* bring the increases of the number of the hot spots.[4−6] As a result, SERS intensity is increased as the decreases of *W*. Besides, the enhanced electromagnetic field also is generated as the *D* is increased. It has been known that the electromagnetic field enhancement is maximized when the laser frequency in the SERS measurement is in resonance with the plasmon band frequency.[42] When *D* is increased, the red shift of the plasmon absorption band of Ag NPs causes the stronger resonance, and therefore the SERS intensity is increased. However, the geometrical arrangement of Ag NPs might generate different effects on the SERS enhancement. The geometric factors can produce distinct local field distributions between NPs and therefore lead to different interparticle interaction.[43] The other measurement on SERS enhancement with disk-like shapes of Ag NPs has indicated that the enhancement is up to 50-fold, when the *W*/*D* decreases from 1 to 0.37.[44] The great enhancement in this case might be due to the special disk-shape structure of the Ag NPs with a large fixed *D* (200 nm) and *W* (75−205 nm).

(b) SERS Enhancements of Au NP-t-PLL Films. The Au NPs are known to be high biocompatible materials. Therefore, we have also detected the SERS enhancement of R6G (1×10^{-6} M) on Au NP-t-PLL films. In our experiments, the limitation of R6G concentration on Ag NPs (1×10^{-9} M) were much lower than that of Au NPs (1×10^{-6} M). To estimate the enhancement factor (EF) for metal NP-t-PLL films, the following expression is applied: $EF = [M_f]/[M_{ads}] \times [I_{SERS}]/[I_{Raman}]$, where M_f is the concentration of the molecules in the bulk sample (used in the Raman experiment), M_{Ads} is the concentration of the adsorbed molecules on the metal surface, and I_{SERS} and I_{Raman} are the intensities of a certain vibration in SERS and Raman spectra, respectively.[45] For SERS of the R6G molecule adsorbed on NPs, the estimated concentration of R6G on the surface based on the presence of a monolayer on the surface was 1×10^{-6} and 1×10^{-9} M for gold and Ag NPs, respectively, compared to the Raman scattering of 1×10^{-2} M R6G dried on bulk sample. Therefore, the EF of 1×10^4 and 1×10^7 was calculated for the vibration of C−C stretching bands at 1650 cm^{-1}. The SERS signal of R6G on the Ag NP-t-PLL film was about three orders stronger than that on the Au NP-t-PLL film. However, the resulting large enhancement factors suggested that both Ag and Au NP-t-PLL films can indeed serve as robust substrates for carrying out molecular sensing with high sensitivity and specificity.

In conclusion, we have successfully prepared a soft SERS substrate based on a 3D structure of biocompatible t-PLL brush conjugated with Ag NPs (Ag NP-t-PLL film). The significant increases of SERS enhancements have been found as *W*/*D* was decreased from 0.9 to 0.2. Because of soft and biocompatibility of t-PLL brush, the films have offered great advantages for the uses for cell or bacterial cultivation. Currently, the identification of cultivated *E. coli* and PC-12 cells is being performed on Ag NP-t-PLL films using SERS. The SERS spectra have been clearly obtained. However, the interpretation of the SERS results is still in progress and will be discussed elsewhere.

Acknowledgment. This study was financially supported by the Taiwan National Science and Technology Program for Nanoscience and Nanotechnology, National Science Council, National Taiwan Normal University, and Genomics Research Center and Institute of Atomic and Molecular Science at Academia Sinica.

References and Notes

(1) Michaels, A. M.; Nirmal, M.; Brus, L. E. *J. Am. Chem. Soc.* **1999**, *121*, 9932–9939.
(2) Xu, H. X.; Bjerneld, E. J.; Käll, M.; Börjesson, L. *Phys. Rev. Lett.* **1999**, *83*, 4357–4360.
(3) Kneipp, K.; Kneipp, H.; Itzkan, I.; Dasari, R. R.; Feld, M. S. *Chem. Rev.* **1999**, *99*, 2957–2976.
(4) Jiang, J.; Bosnick, K.; Maillard, M.; Brus, L. *J. Phys. Chem. B* **2003**, *107*, 9964–9972.
(5) Nie, S.; Emory, S. R. *Science* **1997**, *275*, 1102–1106.
(6) Kneipp, K.; Wang, Y.; Kneipp, H.; Perelman, L. T.; Itzkan, I.; Dasari, R.; Feld, M. S. *Phys. Rev. Lett.* **1997**, *78*, 1667–1670.
(7) Weiss, A.; Haran, G. *J. Phys. Chem. B* **2001**, *105*, 12348–12354.
(8) Xu, M.; Dignam, M. J. *J. Chem. Phys.* **1994**, *100*, 197–203.
(9) Garciá-Vidal, F. J.; Pendry, J. B. *Phys. Rev. Lett.* **1996**, *77*, 1163–1166.
(10) Baumberg, J. J.; Kelf, T.; Sugawara, Y.; Cintra, S.; Abdelsalam, M.; Bartlett, P. N.; Russell, A. E. *Nano Lett.* **2005**, *5*, 2262–2267.
(11) Bell, S. E. J.; Sirimuthu, N. M. S. *J. Am. Chem. Soc.* **2006**, *128*, 15580–15581.
(12) Domke, K. F.; Zhang, D.; Pettinger, B. *J. Am. Chem. Soc.* **2007**, *129*, 6708–6709.
(13) Wei, Y.; Cao, C.; Jin, R.; Mirkin, C. A. *Science* **2002**, *297*, 1536–1540.
(14) Stokes, R. J.; Macaskill, A.; Lundahl, P. J.; Smith, W. E.; Faulds, K.; Graham, D. *Small* **2007**, *3*, 1593–1601.
(15) Moore, B. D.; Stevenson, L.; Watt, A.; Flitsch, S.; Turner, N. J.; Cassidy, C.; Graham, D. *Nat. Biotechnol.* **2004**, *22*, 1133–1138.
(16) Premasiri, W. R.; Moir, D. T.; Klempner, M. S.; Krieger, N.; Jones, G., II; Ziegler, L. D. *J. Phys. Chem. B* **2005**, *109*, 312–320.
(17) Huang, X.; El-Sayed, I. H.; Qian, W.; El-Sayed, M. A. *Nano Lett.* **2007**, *7*, 1591–1597.
(18) Yu, Q.; Guan, P.; Qin, D.; Golden, G.; Wallace, P. M. *Nano Lett.* **2008**, *8*, 1923–1928.
(19) Njoki, P. N.; Lim, I.-I. S.; Mott, D.; Park, H.-Y.; Khan, B.; Mishra, S.; Sujakumar, R.; Luo, J.; Zhong, C.-J. *J. Phys. Chem. C* **2007**, *111*, 14664–14669.
(20) Tie, W.; Hu, X.; Dong, S. *J. Phys. Chem. B* **2006**, *110*, 16930–16936.
(21) Stewart, M. E.; Anderton, C. R.; Thompson, L. B.; Maria, J.; Gray, S. K.; Rogers, J. A.; Nuzzo, R. G. *Chem. Rev.* **2008**, *108*, 494–521.
(22) Wang, H. H.; Liu, C. Y.; Wu, S. B.; Liu, N. W.; Peng, C. Y.; Chan, T. H.; Hsu, C. F.; Wang, J. K.; Wang, Y. L. *Adv. Mater.* **2006**, *18*, 491–495.

(23) Tao, A.; Kim, F.; Hess, C.; Goldberger, J.; He, R.; Sun, Y.; Xia, Y.; Yang, P. *Nano Lett.* **2003**, *3*, 1229–1233.
(24) Chattopadhyay, S.; Lo, H. C.; Hsu, C. H.; Chen, L. C.; Chen, K. H. *Chem. Mater.* **2005**, *17*, 553–559.
(25) Goulet, P. J. G.; dos Santos, D. S., Jr.; Alvarez-Puebla, R. A.; Oliveira, O. N., Jr.; Aroca, R. F. *Langmuir* **2005**, *21*, 5576–5581.
(26) Lu, Y.; Liu, G. L.; Lee, L. P. *Nano Lett.* **2005**, *5*, 5–9.
(27) Merican, Z.; Schiller, T. L.; Hawker, C. J.; Fredericks, P. M.; Blakey, I. *Langmuir* **2007**, *23*, 10539–10545.
(28) Kao, P.; Malvadkar, N. A.; Cetinkaya, M.; Wang, H.; Allara, D. L.; Demirel, M. C. *Adv. Mater.* **2008**, *20*, 3562–3565.
(29) Kim, K.; Lee, H. S.; Kim, N. H. *Anal. Bioanal. Chem.* **2007**, *388*, 81–88.
(30) Kim, K.; Park, H. K.; Kim, N. H. *Langmuir* **2006**, *22*, 3421–3427.
(31) Erol, M.; Du, H.; Sukhishvili, S. *Langmuir* **2006**, *22*, 11329–11336.
(32) Schwartzberg, A. M.; Grant, C. D.; Wolcott, A.; Talley, C. E.; Huser, T. R.; Bogomolni, R.; Zhang, J. Z. *J. Phys. Chem. B* **2004**, *108*, 19191–19197.
(33) Jarvis, R. M.; Goodacre, R. *Anal. Chem.* **2004**, *76*, 40–47.
(34) Wang, Y.; Chang, Y. C. *Langmuir* **2002**, *18*, 9859–9866.
(35) Wang, Y.; Chang, Y. C. *Macromolecules* **2003**, *36*, 6511–6518.
(36) Wu, J. C.; Wang, Y.; Chen, C. C.; Chang, Y. C. *Chem. Mater.* **2008**, *20*, 6148–6156.
(37) Kranz, B. R.; Thiel, E.; Thierfelder, S. *Blood* **1989**, *73*, 1942.
(38) Hildebrandt, P.; Stockburger, M. *J. Phys. Chem.* **1984**, *88*, 5935–5944.
(39) Wang, Y. L.; Chen, H. J.; Wang, E. K. *Nanotechnology* **2008**, *19*, 105604–105608.
(40) Ko, H.; Singamaneni, S.; Tsukruk, V. V. *Small* **2008**, *4*, 1576–1599.
(41) Moskovits, M. *J. Raman Spectrosc.* **2005**, *36*, 485–496.
(42) Ghosh, S. K.; Pal, T. *Chem. Rev.* **2007**, *107*, 4797–4862.
(43) Su, K. H.; Wei, Q. H.; Zhang, X.; Mock, J. J.; Smith, D. R.; Schultz, S. *Nano Lett.* **2003**, *3*, 1087–1090.
(44) Gunnarsson, L.; Bjerneld, E. J.; Xu, H. X.; Petronis, S.; Kasemo, B.; Käll, M. *Appl. Phys. Lett.* **2001**, *78*, 802–804.
(45) Nikoobakht, B.; Wang, J.; El-Sayed, M. A. *Chem. Phys. Lett.* **2002**, *366*, 17–23.

JP903664U